INVESTIGATING ENDWALL-BLADE FILLET RADIUS VARIATION TO REDUCE SECONDARY FLOW LOSSES

Craig Hawes, Richard Williams and Grant Ingram

School of Engineering and Computing Sciences, University of Durham, Durham, DH1 3LE, UK,
craig.m.hawes@gmail.com,r.j.williams5@durham.ac.uk,g.l.ingram@durham.ac.uk

ABSTRACT

In turbomachinery the joint between a turbine blade and the endwall often involves a fillet. Previous studies show that this fillet significantly influences the secondary flows despite regularly being omitted from simulation and testing, specifically that a uniform fillet radius of 16% axial chord increased endwall losses by 10%. It was proposed that a variable radius fillet could reduce secondary flows and the associated endwall losses. This paper describes a computational study to determine what variable radius fillet is required for optimal performance in the cascade. The variable radius fillet ranges from 0.5% to 16% of axial chord and was found using a genetic algorithm optimisation. Although this is a computational study the design offers physically plausible mechanisms by which the extra losses introduced by fillets may be reduced. This paper also suggests a generalised rule of fillet radius variation to minimise endwall losses. A large radius is required on the leading edge that reduces slowly along the pressure side but rapidly on the suction side such that the smallest permitted radius is applied to the suction side. A medium radius is required at the trailing edge.

NOMENCLATURE

C_{ax}	% of axial chord
C_{P0}	Total pressure loss coefficient
C_P	Static pressure coefficient
C_{SKE}	Coefficient of secondary kinetic energy
D	Driver radii
L	Distance between driver radii
n	Normal to flow streamline velocity
P	Pressure
R	Fillet radius
$\dot{S}_{Vol}$	Rate of entropy generation
T	Temperature
V	Velocity
x	Coordinate between drivers
λ	Thermal conductivity
ρ	Density
τ	Shear stress
Subscripts	
mid	Mid-span
r	Radial
sec	Secondary
ups	Upstream

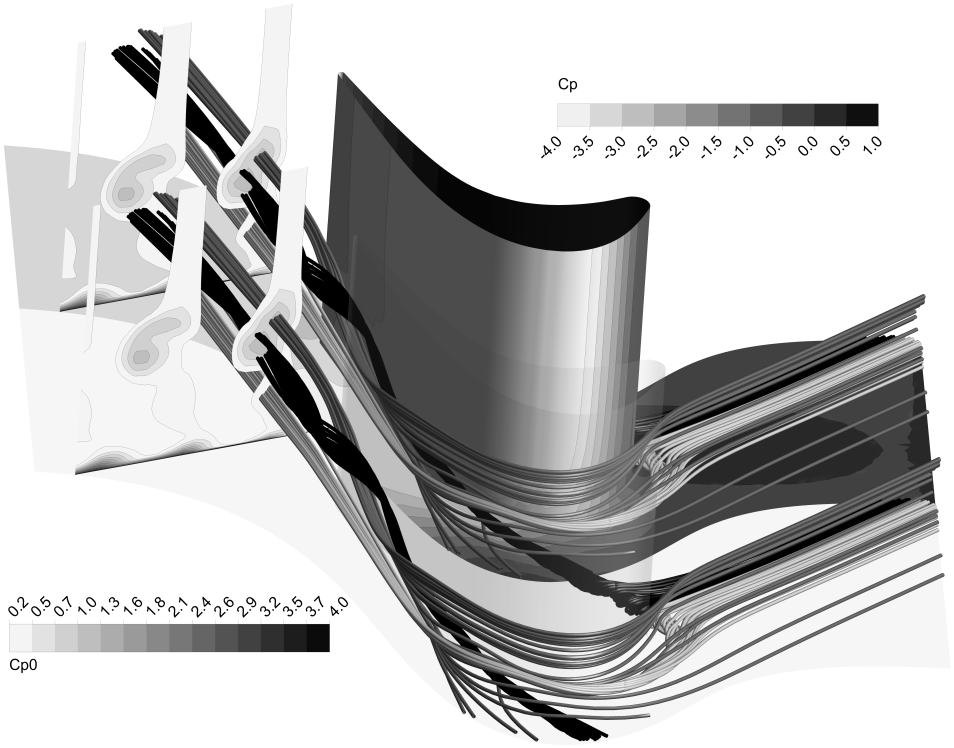

Figure 1: **Secondary Flow Features**

INTRODUCTION

Every real turbomachinery blade has a fillet around its base and yet in many research cascades or simulations the fillet is omitted for simplification.

Denton [1993] provided a comprehensive overview of the factors influencing loss in turbomachines and reported that loss was often divided into three components: profile loss (associated with blade boundary layers), secondary or endwall loss (associated with secondary flows) and leakage losses. In reality the loss sources are seldom independent but in many machines each can account for ⅓ of the loss. This study does not feature a tip clearance and fillet radii have have an extremely limited influence on profile loss as this is driven by the two dimensional aerodynamics of the blade. The only loss source that this variable fillet radii addresses is therefore the secondary or endwall loss.

Secondary Flow

There are a number of different definitions for secondary flow. The simplest explanation is to define secondary flow as any flow, which is not in the primary or ideal streamwise direction. Thus it does not use the maximum amount of its energy to produce work (rotation or thrust).

Sieverding [1985] and Langston [2001] give a review of several models and a summary of the progress in understanding the effects of secondary flows in turbine blade passages. The actual form of this secondary flow is highly complex but there are three main features: The Passage Vortex, the Horseshoe Vortex and the Corner Vortex.

The Passage Vortex is the dominant feature of secondary flow within the blade passage and can be seen in numerous experimental results (Sieverding and Bosche [1983], Gregory-Smith and Graves [1983], Moustapha et al. [1985], Moore and Adhye [1985], Hodson and Dominy [1987] and Harrison [1990] to list just a few.) The passage vortex is formed across the blade passage, the cross passage pressure gradient (from the suction surface of the blade to the pressure surface) affects both the bound-

ary layer fluid and the mid-span flow. The endwall boundary layer velocities are slower relative to the mid-span flow, and therefore follow a tighter radius of curvature. A tangential flow across the passage is created and to preserve continuity, a vortex is formed.

The Horseshoe Vortex is formed at the leading edge of a blade and is produced when the inlet boundary layer meets the blunt leading edge of the blade. The mainstream flow has a higher stagnation pressure than that of the flow nearer the endwall and hence a radial pressure gradient is formed on the blade leading edge. This results in the formation of a vortex structure which moves tangentially around both sides of the leading edge. This feature is described in great detail in Eckerle and Langston [1987].

The Corner Vortex, or sometimes known as the Counter Vortex, is caused by the cross flow underneath the passage vortex interacting with the blade suction surface in a similar manner to the horseshoe vortex. The feature is relatively small compared to the other vortical structures and is only present in experiments with high turning flows.

Fig. 1 taken from the later CFD calculations in the paper provides an illustration of the secondary flows encountered in the cascade. Figure 1 shows the flow around two blades and inside one passage. One blade is illustrated with contours of C_P and the foreground blade is transparent so that the internal passage flows can be visualised. Downstream of each blade a cut plane showing contours of C_{p0} is displayed. The secondary flows are illustrated by streamlines shaded by location. The horseshoe vortex at each leading edge can clearly be seen and Fig. 1 shows how the pressure side of the horseshoe vortex crosses the blade passage to become part of the passage vortex leading to the loss core in the C_{P0} cut-plane. The corner vortex is not illustrated by streamlines but the effect of this feature can be seen at the base of the C_{P0} cut plane.

Despite being a simplification of the real turbine the secondary flow in a cascade is still highly complex and the flow features illustrated in Fig 1 can be found in real machines.

Previous Work

Previous studies on the effect of leading edge modification and endwall fillets include Zess and Thole [2002] who examined the influence of a large fillet at the leading edge of the turbine blade. Lethander and Thole [2004] conducted an optimisation study to determine an optimum fillet pattern for heat transfer using a linear fillet geometry. They found that the optimum fillet was very large at the leading edge and on the pressure side but much smaller on the suction side and around the trailing edge. Lethander's fillet showed similar levels of aerodynamic performance and achieved the design aim of a reduction in thermal loading of around 6%. Lethander's work is the published work that is most similar to this paper but Lethander focuses on heat transfer rather than aerodynamic performance and conducts his optimisation on a turbine vane geometry with around 72° of turning rather than the 110° used in the current study.

Fillets have been considered in conjunction with other technologies, for example Germain et al. [2008] produced a design of profiled endwalls that explicitly included fillet radii and these endwalls were subsequently tested in the LISA rig at ETH Zurich. With fillet radii in the CFD modelling the agreement between predicted and actual performance was much poorer.

More recently Turgut and Camci [2012] examined a leading edge fillet (similar to those used by Zess and Thole [2002]) and nonaxisymmetric endwalls. Turgut and Camci [2013] then continued the work to examine the influence of rim seal flows. The authors showed reductions of up to 15% in area averaged loss with the greatest gains coming from a combination of leading edge fillets and contoured endwalls. However the focus of the paper was the combined benefits of the two technologies and not simply on the influence of a typically fillet radii applied to a turbine stage. A more comprehensive review of fillet radii studies can be found in Mank [2013].

The present work follows on from that of Mank [2013] and Mank et al. [2014] who showed that a

fillet had considerable effect on the secondary flows near the endwall. A large uniform fillet of radius 16% C_{ax} increased loss by 10% compared to no fillet in low speed linear cascade tests.

Mank et al. [2014] identified a number of secondary flow interactions that arise when fillet radii were applied to a sharp-edged cascade. These include: a reduction in the strength of the horseshoe vortex at formation, a larger radial migration of secondary flow, a subsequent increased interaction between the passage vortex and the suction side horseshoe vortex, a trailing edge separation at the fillet and the elimination of the corner vortex.

Mank et al. [2014] suggested that varying the radius of the fillet around the aerofoil could deliver reductions in loss caused by the fillet and have the potential for improvement compared to having no fillet. The contribution this paper makes is to present the design and analysis of such a variable fillet radii.

MEASURES OF LOSS OR ENTROPY GAIN

The secondary kinetic energy from a CFD simulation can be expressed as a non-dimensional Coefficient of Secondary Kinetic Energy (C_{SKE}):

$$C_{SKE} = \frac{V_r^2 + V_{sec}^2}{V_{ups}^2} \tag{1}$$

V_r is the radial component of velocity and V_{sec} is a tangential component of velocity defined by reference to a two dimensional mid-span, Ingram [2003] contains the full definition. Another measure of loss is the total pressure loss coefficient C_{P0}:

$$C_{P0} = \frac{P_{total_{ups}} - P_{total}}{\frac{1}{2}\rho V_{ups}^2} \tag{2}$$

As Denton [1993] argued entropy is the best measure of performance degradation in turbomachines. In the low speed case this is directly related to pressure loss coefficient C_{P0}.

The difficulty in using entropy or C_{P0} in optimisation is that CFD results do not capture the small changes in loss introduced by design perturbations very well. As a result many authors have used proxies for loss that are better predicted by CFD and can more clearly drive the objective function towards the design optimum. For example Bergh et al. [2012], Bagshaw et al. [2008] use C_{SKE}, Germain et al. [2008] used a combination of loss and C_{SKE} and McIntosh et al. [2011] compared a number of objective functions. If more accurate CFD solutions of turbomachinery components become available then these proxies may be discarded.

However the Entropy Generation Rate per unit volume, $\dot{S}_{Vol}$ gives an excellent visualisation of the loss generation in the CFD prediction and can be used as a very valuable tool in examining design trade-offs. This was ably demonstrated by Grewe et al. [2014] who sets the current standard for CFD interpretation. Equation 3 shows how the rate of entropy generation is related to the rate of change of velocity (V) with regards to the velocity normal (n). This indicates a flow with increased vorticity and where flow direction constantly changes would have higher entropy generation.

$$\dot{S}_{Vol} = \frac{\tau}{T}\frac{dV}{dn} + \frac{\lambda}{T}\frac{dT}{dn}^2 \tag{3}$$

TEST CASE

The geometry used is that of the Durham Cascade described in Table 1. This is a well known test case and the geometry can be seen in Figure 1. The largest possible fillet for this geometry was $30\,\mathrm{mm}$ limited by maximum cascade blade separation and the smallest was $1\,\mathrm{mm}$ limited by feasible construction. The inlet boundary layer is turbulent with a shape factor of around 1.2 and a

Inlet Flow Angle	42.8°
Blade Exit Angle	-68.7°
Total Blade Turning Angle	111.5°
Blade Axial Chord Length	$181\,\mathrm{mm}$
Blade Pitch	$191\,\mathrm{mm}$
Blade Span	$375\,\mathrm{mm}$
Re	4×10^5

Table 1: **Cascade Blade Details**

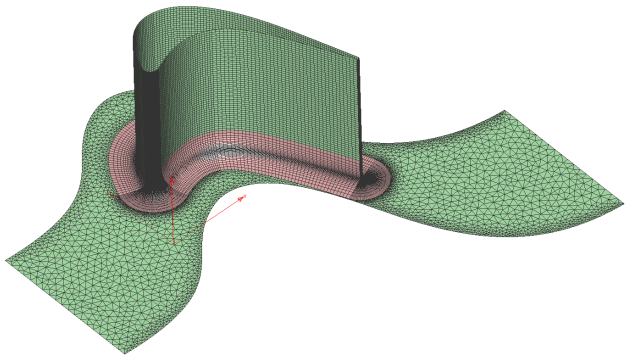

Figure 2: Surface Mesh

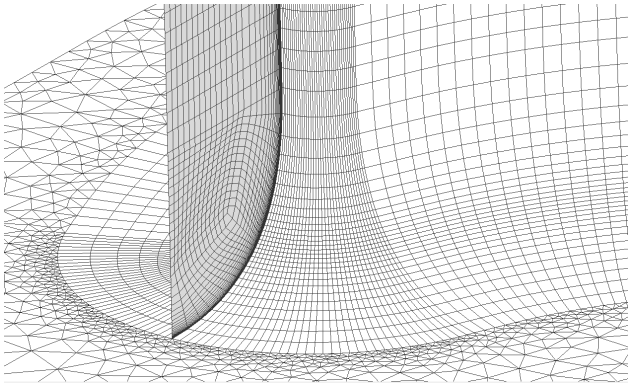

Figure 3: Mesh structure at LE

displacement thickness of around $4\,\mathrm{mm}$. The cascade has been studied for a number of years and is notable in featuring significant areas of transitional flow over the blades and endwalls Förster et al. [2011].

The optimisation method used was a genetic algorithm implemented in the GNU Octave program. The algorithm had a population of 12 chromosomes in each generation and ran for 100 generations. A standalone PC ran the majority of algorithm functions including writing simulation scripts, chromosome selection and calculating cost. The CFD simulations were run on the Durham high performance computing cluster known as Hamilton. The genetic algorithm code was a development of that published by McIntosh et al. [2011] and Hilfer et al. [2012].

The objective function used is shown in Equation 4. The cost function is much simpler than that found in earlier work being proportional to only C_{SKE} where k is a constant. Previous work had show that fillets enhanced the secondary flow and C_{SKE} so an objective function that decreases with decreasing secondary flow was felt to be appropriate. The later results show that flow turning was not altered in the present study so for the present case a simple cost function was appropriate.

$$COST = k \times C_{SKE} \tag{4}$$

Mesh

The mesh used was created in Pointwise version 17.1 R4. The radius variations were all symmetric (i.e. the radial radius equals its perpendicular counterpart). The genetic algorithm wrote a mesh script for each chromosome in the genetic algorithm in Glyph II (the Pointwise scripting language) that was then run on a cluster to create the mesh. Previous CFD work (McIntosh et al. [2011]) showed 600,000 cells were acceptable for simulation of the Durham cascade, there were 1.65 million cells in the present mesh, the number was increased largely due to the complexity of the fillet mesh. Figure 2 shows the structured cells around the blade surface & fillet and unstructured cells at the endwall.

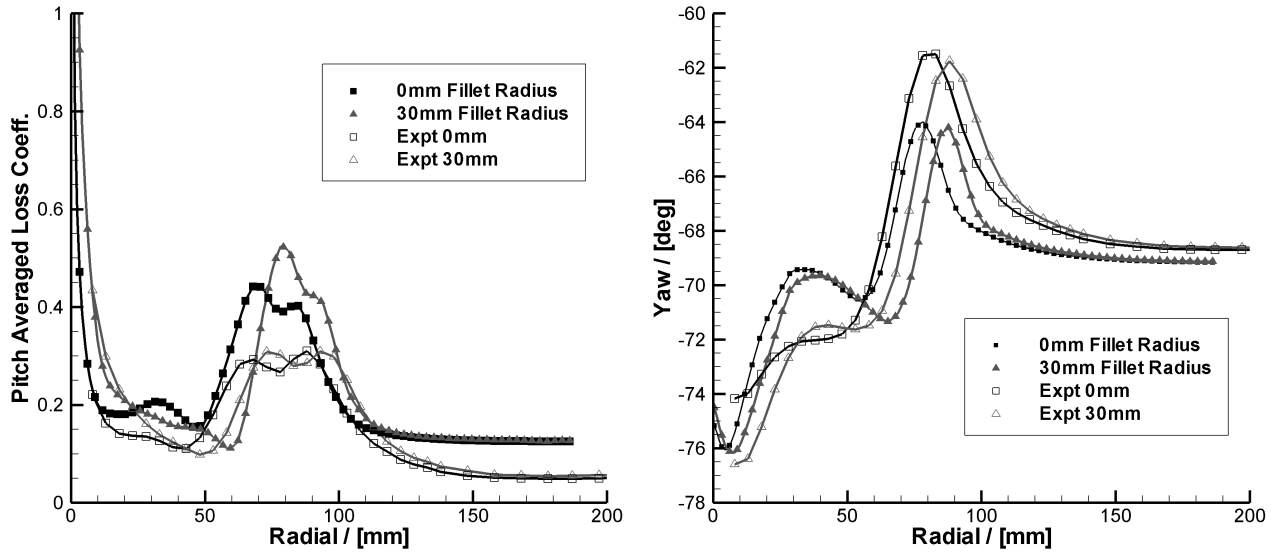

(a) C_{P0} (b) Yaw Angle

Figure 4: **Pitch Averaged CFD vs Experiments at 128%** C_{ax}

Prismatic cells extruded out from the unstructured mesh filled the freestream.

To vary the fillet radius the Genetic Algorithm controlled the radius around the fillet at nine "driver radii" points. The driver radii locations were carefully selected as the minimum number required to allow the widest possible design space. The locations of the driving radii are shown in Figure 5 marked with red dots. At any point between driver radii (D) the fillet radius (R) at a distance x from D_1 is given as a second order dependant curve shown in Equation 5 to ensure smooth variation in radius across driver points i.e. avoiding sharp angles at the drivers. The equation was based on the two adjacent driver radii (D_1 & D_2), L is the distance between the two drivers and K is a smoothing constant.

$$R = D_1 + \left(\frac{D_2 - D_1}{L}\right)\left(K\left(x - \frac{D_2 - D_1}{2}\right)^2 + 1\right) \tag{5}$$

The design of the mesh must be acceptable for all possible radius variations. Figure 3 shows the cross section of a block adjacent to the fillet. The number of cells does not change with respect to the fillet radius however the shape of the cells does. The script is designed to maintain an even cell length along the curve adjacent to the fillet and ensures cells meet simulation requirements for aspect ratio and skew for any possible radius.

Because of the variation in the radius it was difficult to create a uniform fillet surface that stuck to the intended geometry and initially a pronounced "bulging" effect occurred around the fillet. This problem was most noticeable around the LE and TE as the fillet turns sharply through a large radial angle but did occur all over the fillet. The problem was overcome by increasing the number of divisions in the fillet surface such that the surface could be more tightly controlled as shown in Figure 3.

CFD Computation

The CFD follows simulation parameters as previously validated for the Durham Cascade. Fluent version 14.1 was used as the solver with a pressure-based transition Shear-Stress Transport (SST) k-omega model and default constants.

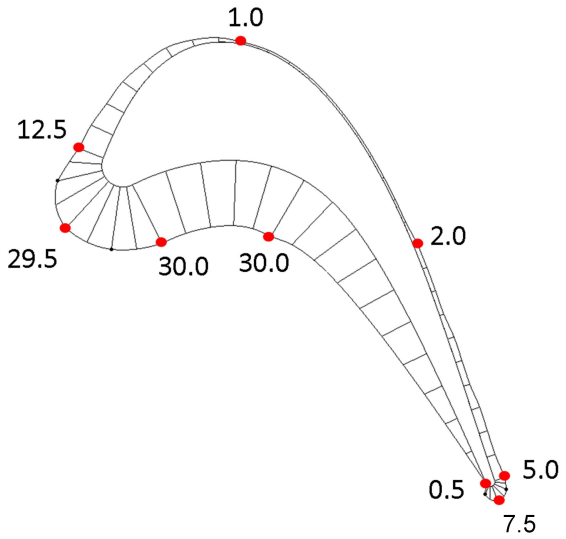

Figure 5: Optimised fillet radius. (Driver radii in mm)

A constant velocity inlet was used in all the computations, since the case is incompressible this gave a constant mass flow. The velocity was set to $19\,\mathrm{m/s}$ with a boundary layer profile based on measurements from the Durham Cascade: turbulence intensity of 5% and length scale of $0.936\,\mathrm{mm}$. The outlet was a pressure outlet and a symmetry plane was applied at mid-span. A periodic boundary was placed on either side of the blade and a no-slip wall boundary made up the blade and endwall surface. Second order upwind discretisation was used with the semi-implicit method for pressure linked equations (SIMPLE).

Convergence criteria for continuity was set as a drop in three orders of magnitude. Acceptable convergence for all other residuals was set at 10^{-4} during the genetic algorithm runs following the approach of McIntosh et al. [2011]. Convergence time was further reduced by interpolating the result of a converged simulation for no fillet at the beginning of each simulation. Figure 4 shows pitch averaged results from the current computation plotted against the experimental results from Mank et al. [2014] for the no fillet $0\,\mathrm{mm}$ and the large fillet $30\,\mathrm{mm}$ case. Despite the use of a transitional model for turbulence the blade wake is not well captured by the CFD but the changes between the large and small fillets in CFD and experiment are comparable. Overall the CFD solution captures changes in flow patterns as well as simulations used in previous work e.g. Bagshaw et al. [2008]. The validation activity therefore provided good confidence in the use of the CFD for the design exercise.

RESULTS

Figure 5 shows a plan view of the final variable radius fillet design. The optimal design features a large fillet at the leading edge and on the pressure side of the blade but a very small radius fillet on the suction side that grows towards the trailing edge. The results are compared to both the $0\,\mathrm{mm}$ fillet radius case and the $30\,\mathrm{mm}$ fillet radius case used by Mank et al. [2014].

Figure 6 illustrates the wall pressure gradient and boundary layer streamlines for the $0\,\mathrm{mm}$ and the optimised case at the leading edge of the blade. Although the optimised fillet keeps the geometrical location of the horseshoe vortex in roughly the same place the vortex intensity (indicated by shading the streamlines by entropy generation rate) is somewhat smaller for the optimised case. Contours on the surface of the blade and endwall in figure 6 show static pressure.

It is notable that the optimisation chose the largest radius possible for the leading edge. The

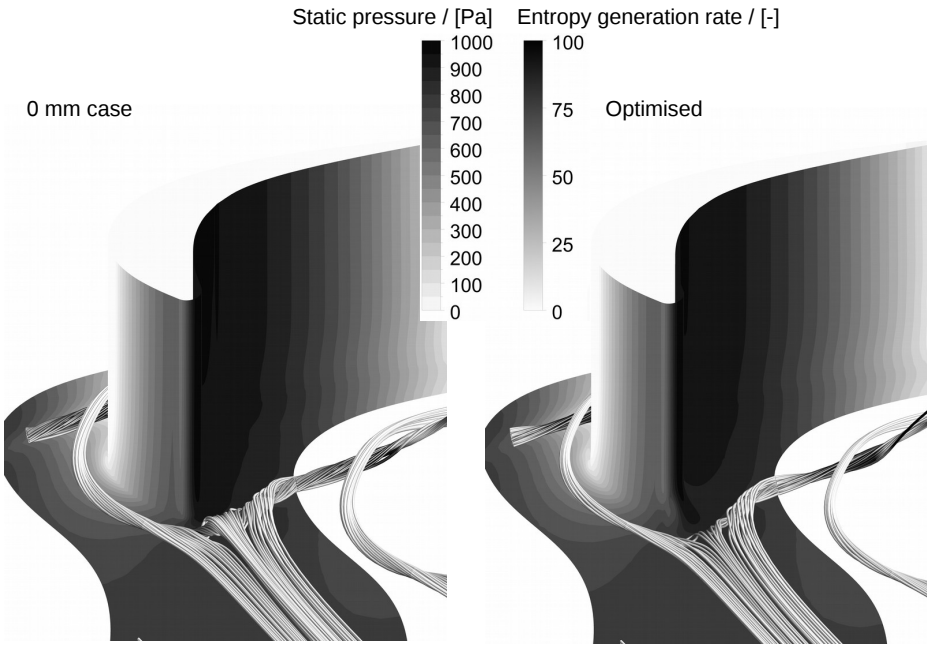

Figure 6: **Streamlines (shaded by $\dot{S}_{Vol}$) at the Leading Edge.**

maximum radius was limited by the throat dimensions of the blade passage and this limitation is used for all points around the blade surface. However it would be possible to have an even larger radius on the leading edge.

In order to further examine the performance of the fillet iso-surfaces and contours of entropy generation rate were generated using post-processing software. This technique (copied from Grewe et al. [2014]) allows the predicted sources of loss to be easily geometrically located. A number of cut planes perpendicular to the locus of trailing edges are shown in Figure 7 for the sharp edged, $30\,\mathrm{mm}$ and optimised case, the scale is logarithmic. The highest values of entropy generation take place on the suction surface boundary layer but this takes place over a very small area so is not immediately visible.

A number of features are clearly apparent:

- The large fillet radius delays the migration of secondary flow across the passage. Despite this significant change in flow structure the entropy generation is of a similar magnitude for all three cases although it is concentrated on the suction surface for the larger fillet. The authors attribute the small changes observed to the fact that fillet radii are a secondary effect on the secondary flows. The primary cause of these flow structures is the overturning of the incoming boundary layer and this mechanism is not changed fundamentally by the application of fillet radii.
- The $0\,\mathrm{mm}$ and optimised fillets show a large loss generating region in the blade endwall junction that is absent for a $30\,\mathrm{mm}$ fillet
- Higher radial migration of the secondary loss cores for the $30\,\mathrm{mm}$ case
- The $30\,\mathrm{mm}$ fillet shows an endwall separation at the trailing edge. This is absent in the optimised and $0\,\mathrm{mm}$ case.

Fillet	$100 \times C_{SKE}$	ΔC_{SKE}	C_{P0}	ΔC_{P0}	Yaw Angle	Inlet C_P
$0\,\mathrm{mm}$ Uniform	1.317	-	0.21779	-	-68.97	3.55
$30\,\mathrm{mm}$ Uniform	1.393	+5.8%	0.22983	+5.5%	-69.30	3.72
Optimised	1.072	-18.6%	0.21697	-0.4%	-68.99	3.54

Table 2: **Area Averaged Results at 128%** C_{ax} **and -100%** C_{ax}

- At the exit the overall picture on all three cases is very similar, although the endwall separation for the $30\,\mathrm{mm}$ case is still visible. As in previous work the $30\,\mathrm{mm}$ fillet shows increased radial migration but the downstream picture with and without the fillets applied is very similar.

These characteristics are very similar to that observed experimentally by Mank et al. [2014] for the sharp and large fillet case.

Figure 8 shows the CFD pitch averaged results for the $0\,\mathrm{mm}$, $30\,\mathrm{mm}$ and optimised fillet designs for C_{P0} and yaw angle. The most remarkable feature is how the optimal design matches the $0\,\mathrm{mm}$ closely - the optimised fillet has not improved over the sharp edged case.

Table 2 shows both C_{SKE} and C_{P0} area averaged results 28% of an axial chord downstream of the trailing edge. The last column shows the area averaged C_P at the inlet plane (located at -100% C_{ax}). The design intention to minimise C_{SKE} has clearly been achieved. The loss results show that the predicted loss for the optimal case is similar to the un-filleted case - so an optimal fillet has not been able to improve on the zero fillet case but instead has recovered the performance lost by introducing a uniform fillet around the blade.

The increase in average predicted C_{P0} from the $0\,\mathrm{mm}$ to $30\,\mathrm{mm}$ fillet of 5.5% is smaller than the experimental change reported by Mank et al. [2014]. However as discussed earlier loss prediction using CFD is challenging and the trend is captured effectively and as shown in the preceding figures is based on physically plausible mechanisms.

In the present study the only geometry change was to apply fillets to the blade and the inlet velocity (and so the mass-flow) was kept constant. If the area changes introduced by fillet radii were significant the inlet static pressure would be increased. Table 2 shows that the inlet C_P value for the optimised case is very close to the $0\,\mathrm{mm}$ case but the operating point of the cascade has been moved slightly for the $30\,\mathrm{mm}$ case. In a real design scenario the blade pitch could be adjusted to bring the cascade back to the same operating point.

DISCUSSION

Overall the design proposed in Figure 5 is strikingly similar to that proposed by Lethander and Thole [2004]. The blade in this paper has a a larger turning angle 110° rather than 72° and the optimisation aims to improve aerodynamics rather than thermal performance. Despite these differences the similarity in the two final geometries suggests that some general criteria may be put forward for reducing the impact of fillet radii. The authors suggest the following general guidelines for radius size around the blade:

- A large radius on the leading edge and into the pressure side of the blade: this reduces the entropy generation rates found in the horseshoe vortex formation and limits its size.

- A gently decreasing radius from the leading edge to the suction side: this limits suction side horseshoe vortex growth.

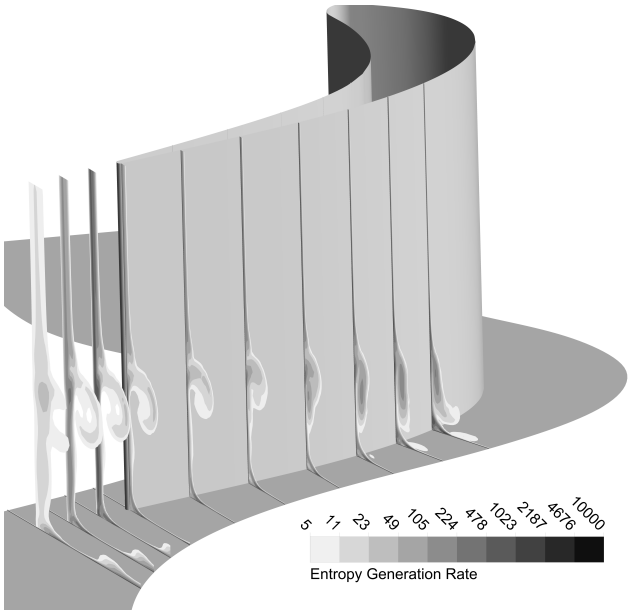

(a) 0 mm

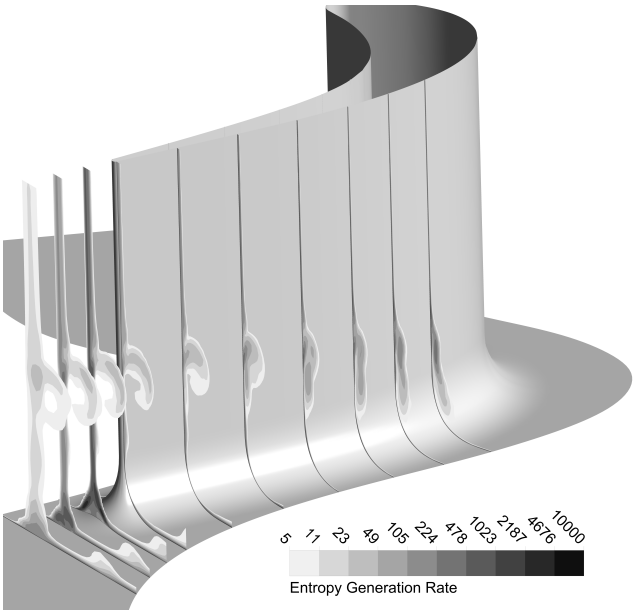

(b) 30 mm

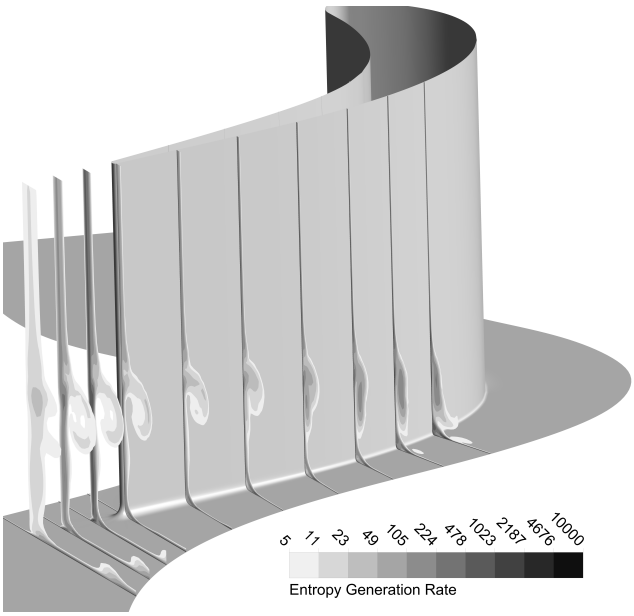

(c) Optimised

Figure 7: **Contours of Entropy Generation Rate** $\dot{S}_{Vol}/[-]$

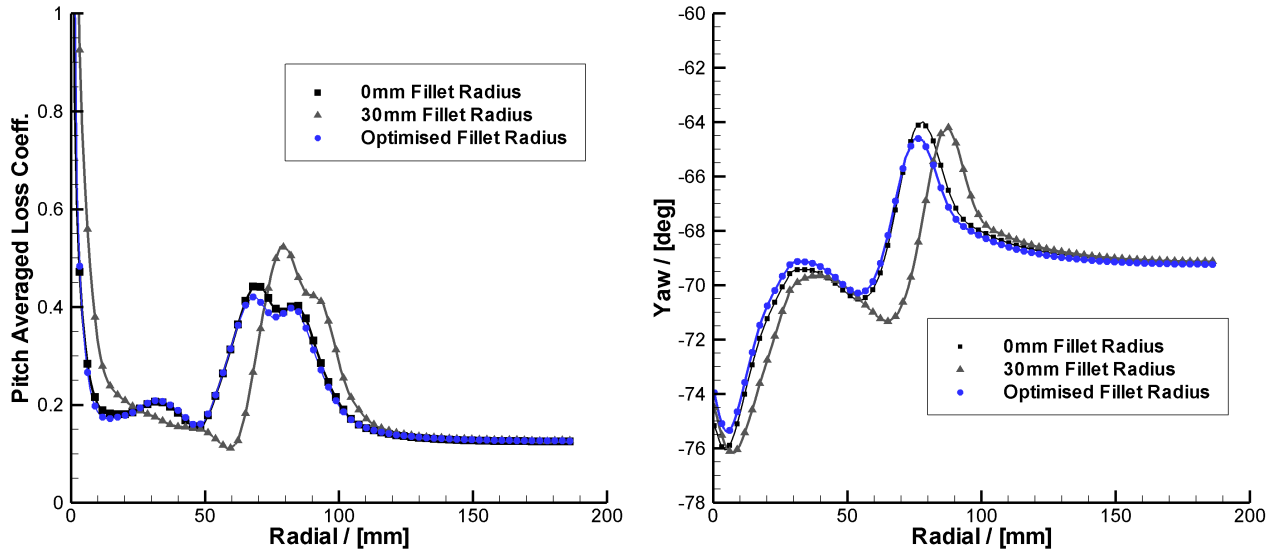

(a) C_{P0} (b) Yaw Angle

Figure 8: **Pitch Averaged Optimised vs Baseline at 128% C_{ax}**

- The smallest radius possible on the suction side: this limits the migration of secondary flows up the blade span.
- A medium radius at the trailing edge: a uniform large radius at the trailing edge has been shown to separate and careful choice of trailing edge geometry will remove this feature.

However these recommendations come with some caveats, the current study has an arbitrary minimum fillet radius of $1\,\mathrm{mm}$ or some 0.5% of C_{ax}. This limit is based on cascade manufacture considerations and has not been scaled from real world geometries. It may be that the minimum fillet radius that can be obtained in practise is larger than this - the present study suggests that fillets should be as small as possible on the suction side but further work is required to determine the trade-offs resulting from a larger minimum radius.

CONCLUSIONS

The computational method used was bench-marked against recent experimental measurements by Mank et al. [2014] and found to give reasonable predictions of the trends that occur when fillets are applied to the cascade.

A genetic algorithm optimisation was created to investigate the effect of varying the radius of the fillet around the blade endwall junction on the aerodynamic performance of a low speed linear cascade. A candidate design was obtained and the final CFD results analysed in detail.

The optimised design demonstrated a similar value of averaged C_{P0} as the sharp edged case and a reduction in C_{P0} of 5.5% compared to the $30\,\mathrm{mm}$ fillet. The objective function used was the secondary kinetic coefficient. The optimised design therefore does not reduce predicted loss but returns it to the original value before a large radius is applied.

The optimised design features a large leading edge fillet radius and the smallest allowable radius on the suction side. This pattern is similar to that other authors have observed when carrying out optimisation studies on fillet radii and some general design rules are proposed.

The numerical benefits suggested are based on plausible physical processes identified from the

CFD solutions. An experimental campaign is necessary to validate and quantify the loss reductions that are predicted.

REFERENCES

D Bagshaw, DG Gregory-Smith, GL Ingram, M Stokes, and N Harvey. The design of three dimensional turbine blades combined with profiled endwalls. *Proc. I.Mech.E. Series A: J. Power and Energy*, 2008.

J Bergh, G Snedden, and C Meyer. Optimisation of non-axisymmetric end wall contours for the rotor of a low speed, 1 1/2 stage research turbine with unshrouded blades. *GT2012-68569*, 2012.

JD Denton. The 1993 IGTI scholar lecture: Loss mechanisms in turbomachines. *Transactions of the ASME, Journal of Turbomachinery*, 115(4):621–656, 1993.

WA Eckerle and LS Langston. Horseshoe vortex formation around a cylinder. *Transactions of the ASME, Journal of Turbomachinery*, 109:278–285, April 1987.

F Förster, DB Sims-Williams, GL Ingram, and RG Dominy. Time resolved measurements in the durham cascade. *GT2011-45838*, 2011.

T Germain, M Nagel, I Raab, P Schuepbach, RS Abhari, and MG Rose. Improving efficiency of a high work turbine using non-axisymmetric endwalls part I: Endwall design and performance. *GT2008-50469*, 2008.

DG Gregory-Smith and CP Graves. Secondary flows and losses in a turbine cascade. *AGARD-CP-351, AGARD Conference Proceedings No. 351: Viscous Effects in Turbomachines*, 1983.

RP Grewe, RJ Miller, and HP Hodson. The effect of endwall manufacturing variations on turbine performance. *GT2014-25326*, 2014.

S Harrison. The influence of blade lean on turbine losses. *ASME 90-GT-55*, 1990.

M Hilfer, GL Ingram, and SI Hogg. Endwall profiling with tip clearance flows. *GT2012-68488*, 2012.

HP Hodson and RG Dominy. The off-design performance of a low-pressure turbine cascade. *Transactions of the ASME, Journal of Turbomachinery*, 109:201–209, 1987.

GL Ingram. *Endwall Profiling for the Reduction of Secondary Flow in Turbines*. PhD thesis, School of Engineering, University of Durham, 2003.

LS Langston. Secondary flows in axial turbines-a review. *Annals of the New York Academy of Sciences: Heat Transfer in Gas Turbine Systems*, 2001.

AT Lethander and KA Thole. Vane-endwall junction optimisation to reduce turbine vane passage and adiabatic wall temperatures. *Journal of Propulsion and Power*, 20(6):1105–1116, 2004.

S Mank. An experimental investigation on the effect of fillet radii on secondary flow structures in a turbine cascade. Master's thesis, Universität Stuttgart, Institut für Luftfahrtantriebe (ILA), 2013.

S Mank, M Hilfer, RJ Williams, SI Hogg, and GL Ingram. Secondary flows and fillet radii in a linear turbine cascade. *GT2014-25458*, 2014.

J McIntosh, R MacPherson, GL Ingram, and SI Hogg. Profiled endwall design using genetic algorithms with different objective functions. *GT2011-45836*, 2011.

J Moore and RH Adhye. Secondary flows and losses downstream of a turbine cascade. *Transactions of the ASME, Journal of Engineering for Gas Turbines and Power*, 107:961, October 1985.

SH Moustapha, GJ Paron, and JHT Wade. Secondary flows in cascades of highly loaded turbine blades. *Transactions of the ASME, Journal of Engineering for Gas Turbines and Power*, 107: 1031–1038, October 1985.

CH Sieverding. Recent progress in the understanding of basic aspects of secondary flows in turbine blades passages. *Transactions of the ASME, Journal of Engineering for Gas Turbines and Power*, 107:248, 1985.

CH Sieverding and Van Den Bosche. The use of coloured smoke to visualize secondary flows in a turbine-blade cascade. *Journal of Fluid Mechanics, Cambridge University Press*, 134:85–89, 1983.

O Turgut and C Camci. Experimental investigation and computational evaluation of contoured endwall and leading edge fillet configurations in a turbine ngv. *GT2012-69304*, 2012.

O Turgut and C Camci. Influcence of leading edge fillet and nonaxisymmetric contoured endwall on turbine ngv exit flow structure and interactions with the rim seal flow. *GT2013-95843*, 2013.

GA Zess and KA Thole. Computational design and experimental evaluation of using a leading edge fillet on a gas turbine vane. *Transactions of the ASME, Journal of Turbomachinery*, 2002.